From: **Environmental Modeling & Assessment** <lorelie.protacio@springer.com>
Date: Wed, Jan 8, 2014 at 9:52 PM
Subject: Your Submission ENMO-D-13-00080R1
To: Alejandro José Vitale <vitale.alejandro@gmail.com>

Dear Alejandro,

We have received the reports from our advisors on your manuscript, "3D NUMERICAL MODEL OF THE THERMAL INTERACTION BETWEEN SEDIMENT-WATER-ATMOSPHERE", submitted to
Environmental Modeling and Assessment

Based on the advice received, the Editor has decided that your manuscript can be accepted for publication after you have carried out the corrections as suggested by the reviewer(s).

Attached, please find the reviewer's comments for your perusal.

There is additional documentation related to this decision letter. To access the file(s), please click the link below. You may also login to the system and click the 'View Attachments' link in the Action column.

http://enmo.edmgr.com/l.asp?i=20909&l=BVDF2ZZQ

Please submit your revised manuscript online by using
the Editorial Manager system which can be accessed at:

http://enmo.edmgr.com/

Your username is: avitale
Your password is: xxxxxx
I am looking forward to receiving your revised manuscript
before 12 Mar 2014

With kind regards,
Springer
The Editorial Office
P.O. Box 990
3300 AZ DORDRECHT
The Netherlands

Environmental Modeling and Assessment

3D NUMERICAL MODEL OF THE THERMAL INTERACTION BETWEEN SEDIMENT-WATER-ATMOSPHERE

--Manuscript Draft--

Manuscript Number:	ENMO-D-13-00080R1
Full Title:	3D NUMERICAL MODEL OF THE THERMAL INTERACTION BETWEEN SEDIMENT-WATER-ATMOSPHERE
Article Type:	Original Research
Keywords:	3d numerical model; finite-difference method; heat flux; sediment-water-atmosphere; saltmarsh
Corresponding Author:	Alejandro José Vitale, Dr. Instituto Argentino de Oceanografía Bahía Blanca, Buenos Aires ARGENTINA
Corresponding Author Secondary Information:	
Corresponding Author's Institution:	Instituto Argentino de Oceanografía
Corresponding Author's Secondary Institution:	
First Author:	Alejandro José Vitale, Dr.
First Author Secondary Information:	
Order of Authors:	Alejandro José Vitale, Dr.
	María Cintia Piccolo, PhD
	Sibila Andrea Genchi, Dr.
	Claudio Delrieux, Dr.
	Gerardo Miguel Eduardo Perillo, PhD
Order of Authors Secondary Information:	
Abstract:	This paper describes a 3D numerical model of heat flux that employs finite-difference approximation for the simulation, prediction and visualization of sediment, water and air temperature, applied in Villa del Mar saltmarsh, Bahía Blanca Estuary, Argentina. To make this computation, we develop an open-source software tool called Hemera 1.0 which is characterized by having little complexity and low hardware requirements. The model considers three heat transfer processes: diffusion, convection and radiation, using bulk aerodynamic formulas as boundary conditions between the interfaces. The aforementioned model was applied for the month of January 2009. This month was selected because it shows the highest thermal and radiative energy oscillation. The model reproduces adequately the physical processes of the heat balance and showed an adequate response to changes in the boundary conditions. In addition, according to the model design, meteorological and oceanographic data and some soil properties are the only data input used for modeling. It is easily adaptable to other environments such us lakes, lagoons, reservoirs, among others, in order to carry out similar studies.
Response to Reviewers:	Dear Editor-in-Chief, Thank you for your comments and valuable advices about our paper (Number: ENMO-D-13-00080). A new version was submitted. We condensed the manuscript to 27 pages according to its suggestions. Also, linguistic corrections were introduced to the text. With kind regards. Dr. Alejandro J. Vitale.

3D NUMERICAL MODEL OF THE THERMAL INTERACTION BETWEEN SEDIMENT-WATER-ATMOSPHERE

Alejandro J. Vitale [ab*]; M. Cintia Piccolo [ac]; Sibila A. Genchi[a]; Claudio Delrieux [ab]; Gerardo M.E. Perillo[ad]

[a] Instituto Argentino de Oceanografía, CONICET, CC 804, B8000FWB, Bahía Blanca, Argentina.
[b] Departamento de Ingeniería Eléctrica y de Computadoras, Universidad Nacional del Sur, 8000, Bahía Blanca, Argentina.
[c] Departamento de Geografía y Turismo, Universidad Nacional del Sur, B8000, Bahía Blanca, Argentina.
[c] Departamento de Geología, Universidad Nacional del Sur, B8000, Bahía Blanca, Argentina.

[*]Corresponding author: vitale.alejandro@gmail.com
Tel: +54-291-4861112
Fax: +54-291-4861519

ABSTRACT

This paper describes a 3D numerical model of heat flux that employs finite-difference approximation for the simulation, prediction and visualization of sediment, water and air temperature, applied in Villa del Mar saltmarsh, Bahía Blanca Estuary, Argentina. To make this computation, we develop an open-source software tool called *Hemera 1.0* which is characterized by having little complexity and low hardware requirements. The model considers three heat transfer processes: diffusion, convection and radiation, using bulk aerodynamic formulas as boundary conditions between the interfaces. The aforementioned model was applied for the month of January 2009. This month was selected because it shows the highest thermal and radiative energy oscillation. The model reproduces adequately the physical processes of the heat balance and showed an adequate response to changes in the boundary conditions. In addition, according to the model design, meteorological and oceanographic data and some soil properties are the only data input used for modeling. It is easily adaptable to other environments such us lakes, lagoons, reservoirs, among others, in order to carry out similar studies.

KEYWORDS: 3d numerical model; finite-difference method; heat flux; sediment-water-atmosphere; saltmarsh

1. INTRODUCTION

The amount of heat exchanged between adjacent surfaces (e.g., sediment/water-atmosphere) is called heat flux. Heat flux provides the basis for establishing the thermal regime of a given surface. Intertidal areas are spatially complex and temporally dynamic environments [2] that show different patterns from those typically observed at a site which depends entirely on solar radiation [3]. Knowledge regarding heat exchange between sediment, water and atmosphere in these environments (e.g., tidal flat, saltmarsh, beaches) is important for understanding physical and biological processes [15, 23].

Numerical modeling plays an important role in the earth sciences. Analytical solutions of the heat equation are applicable only to uniform systems or simple environments. In

contrast, numerical models are applicable to any type of system or real environments. Therefore, numerical modeling is an essential tool for many environmental studies, because it allows to describe and predict physical processes, particularly in those environments where direct and continuous measurements are costly and complex [44].

There are several previous researches focused on numerical modeling of heat exchange across the water-atmosphere interface in both marine [e.g., 37, 41, 9, 7, 29] and continental environments [e.g., 16, 4, 10, 19, 13]. Many other studies involved the thermal modeling across the sediment-water interface especially in shallow water bodies [e.g., 14, 43, 39, 8, 11, 12] and across the sediment-atmosphere interface [e.g., 40, 26, 27]. However, studies based on modeling of thermal interaction between sediment-water-atmosphere as occurs in coastal areas, are comparatively scarse [e.g., 3, 17, 18, 38, 35, 15, 30, 42, 24]. In this kind of complex interactions, the surface heat is exchanged across the water/sediment-water/atmosphere interfaces, where the magnitude of the temperature changes depends on both existing atmospheric and marine conditions, acting at different temporal scales.

According to several investigations, the temperature of intertidal sediment at shallow depths shows significant fluctuations (e.g., daily, seasonal) depending on parameters such as solar radiation, air temperature, subaerial exposure time, soil properties, etc. Intertidal sediments can absorb and store large amounts of heat [23]; therefore, it is enough to control the heat flux either in the bottom water or above the soil surface. For instance, Sequeira and Piccolo [38] found that soil heat flux is the most important term in the prediction of the water temperature in an intertidal area during low tide.

This paper describes a three-dimensional (3D) numerical model of heat flux that employs finite-difference approximation for the simulation, prediction and visualization of sediment, water and air temperature, applied in Villa del Mar saltmarsh (SVM) (38°51'26" S, 62°07'02" W) Bahía Blanca Estuary, Argentina. The modeling is carried out using an open-source software called *Hemera 1.0* that was developed by the authors. The model considers three heat transfer ways: diffusion, convection and radiation, using bulk aerodynamic formulas as boundary conditions between the sediment-water-atmosphere surfaces. According to the model design, meteorological and oceanographic data and some soil properties are the only data input used for modeling.

2. NUMERICAL METHODS AND SOFTWARE

In this section, we provide a description of the equations used for the processes involved in heat flux jointly with the numerical solution proposed to solve the mathematical model. Also, the software *Hemera 1.0* developed for modeling the heat exchange is presented.

2.1. HEAT EQUATION

The heat transfer parameters over heterogeneous surfaces do not present the same relationship to each other such as could occur in homogeneous surfaces [5]. Consequently, this heterogeneity must be taken into account in the modeling. For this reason, we consider the following general equation of heat diffusion

$$\frac{\partial T}{\partial t} = \nabla_{\bullet}(k_s \nabla T) \tag{1}$$

where T represents the temperature [K] and k_s the thermal diffusivity [m^2 s^{-1}]. Applying the product rule to equation (1) we obtain

$$\frac{\partial T}{\partial t} = \left(\nabla k_s\right)_{\bullet} \left(\nabla T\right) + k_s \left(\nabla^2 T\right) \tag{2}$$

Over homogeneous terrain k_s is constant and, in consequence, the first term in equation 2 is 0, then

$$\frac{\partial T}{\partial t} = 0 + k_s \nabla^2 T \equiv k_s \left[\frac{\partial^2 T}{\partial^2 x} + \frac{\partial^2 T}{\partial^2 y} + \frac{\partial^2 T}{\partial^2 z} \right] \tag{3}$$

2.2. NUMERICAL SOLUTION

There are several numerical approximations that are widely used for solving a model. In this work, the finite-difference method was applied (FDM). FDM has been proved to be reasonably reliable, robust and less computationally intensive for modeling heat exchange between sediment-atmosphere interface [e.g., 40, 26, 1, 21] and water-atmosphere interface in coastal areas [e.g., 34]. In addition, FDM has enormous advantages in terms of computational implementation such as programming and hardware optimization.

Few methods have a favourable performance for the construction of 3D models (e.g., Alternating Direction Implicit (ADI), ADI fully implicit, Duglas-Gunn, Crank-Nicholson and the Euler method). The explicit Euler method was used in the implementation of the model, since it allows a better memory optimization and an efficient parallel implementation, with up to 128 simultaneous tasks, as was in this case.

Press *et al.* [36] described the explicit Euler method as accurate, with an acceptable stability when compared with other methods under the same conditions. Computing speeds using parallel explicit Euler method exceed those obtained with non-parallel implicit methods. The memory required for the calculation is considerably lower than that required for implicit implementations. It is always possible to get the same accuracy with any technique, but penalizing the convergence speed depending on the method employed.

2.2.1. DISCRETE HEAT DIFFUSION

Discretizing the equation of heat diffusion (Eq. 3) using central finite-difference schemes and explicit Euler method, it follows that

$$T^{t+1} = T^t + \left[v_x \delta_x^2 + v_y \delta_y^2 + v_z \delta_z^2 \right] T^t \tag{4}$$

where

$$T^t \equiv T^t_{xyz} \equiv T^t_{ijk} \equiv T(x_i, y_j, z_k; t) \tag{5}$$

$$v_x \equiv k_s \frac{\Delta t}{\Delta x^2}; \qquad v_y \equiv k_s \frac{\Delta t}{\Delta y^2}; \qquad v_z \equiv k_s \frac{\Delta t}{\Delta z^2} \tag{6}$$

$$\delta_x^2 T^t \equiv T_{i-1\,jk}^t - 2T_{ijk}^t + T_{i+1\,jk}^t \tag{7}$$

$$\delta_y^2 T^t \equiv T_{ij-1k}^t - 2T_{ijk}^t + T_{ij+1k}^t \tag{8}$$

$$\delta_z^2 T^t \equiv T_{ijk-1}^t - 2T_{ijk}^t + T_{ijk+1}^t \tag{9}$$

The stability condition, that is, the convergence condition, is given by

$$v_x + v_y + v_z < \frac{1}{2} \tag{10}$$

The thermal diffusivity is not constant, nor analogous for the elements involved in the model (sediment, water and air). The sediments have differences in composition and in level of saturation along a profile crossing an intertidal area. In addition, latent and sensible heat flux is affected by wind at different heights and by turbulence generated by waves. Therefore, changes in diffusivity are required to be considered in the discretization process. Starting from equation (2), applying central finite-difference schemes and using explicit Euler method, it follows that

$$T^{t+1} = T^t + \left[v_x \delta_x^2 + v_y \delta_y^2 + v_z \delta_z^2 \right] T^t + \Delta t \left[\delta_x k_s^t \delta_x T^t + \delta_y k_s^t \delta_y T^t + \delta_z k_s^t \delta_z T^t \right] \tag{11}$$

where

$$k_s^t \equiv k^t \equiv k_{xyz}^t \equiv k_{ijk}^t \equiv k_s(x_i, y_j, z_k; t) \tag{12}$$

$$\delta_x k^t \equiv \frac{k_{i+1\,jk}^t - k_{i-1\,jk}^t}{2\Delta x} \tag{13}$$

$$\delta_y k^t \equiv \frac{k_{ij+1k}^t - k_{ij-1k}^t}{2\Delta y} \tag{14}$$

$$\delta_z k^t \equiv \frac{k_{ijk+1}^t - k_{ijk-1}^t}{2\Delta z} \tag{15}$$

$$\delta_x T^t \equiv \frac{T_{i+1\,jk}^t - T_{i-1\,jk}^t}{2\Delta x} \tag{16}$$

$$\delta_y T^t \equiv \frac{T_{ij+1k}^t - T_{ij-1k}^t}{2\Delta y} \tag{17}$$

$$\delta_z T^t \equiv \frac{T_{ijk+1}^t - T_{ijk-1}^t}{2\Delta z} \tag{18}$$

The equations (4) and (11) allow to model the heat diffusion. This will be applied in a 3D model that involves heterogeneities at both spatial and temporal dimensions. The two basic elements of the model (water and air) have a displacement caused by waves, tidal and wind effects that lead to a heat exchange by convection and conduction. Convective heat (Eq. 19) is modeled by adding a 3D convective term to the heat equation (Eq. 1) [20]

$$\frac{\partial T}{\partial t} = \nabla_{\bullet}(k_s \nabla T - \vec{u}_s \nabla T) \tag{19}$$

$$\vec{u}_s = u(u_x, u_y, u_z) \tag{20}$$

where *u* is the 3D fluid velocity (u_x, u_y, u_z). The equation (19) was also implemented in order to compensate for the heterogeneity of the elements involved in the model. By adding the convective term to equation (11), it follows that

$$\begin{aligned} T^{t+1} = T^t + \left[v_x \delta_x^2 + v_y \delta_y^2 + v_z \delta_z^2 \right] T^t + \Delta t \left[\delta_x k_s^t \delta_x T^t + \delta_y k_s^t \delta_y T^t + \delta_z k_s^t \delta_z T^t \right] ... \\ ... - \Delta t \left[u_x \delta_x T^t + u_y \delta_y T^t + u_z \delta_z T^t \right] \end{aligned} \tag{21}$$

The Courant-Friedrichs-Lewy [6] condition is incorporated into the model. The 3D condition is expressed as

$$\frac{u_x \Delta t}{\Delta x} + \frac{u_y \Delta t}{\Delta y} + \frac{u_z \Delta t}{\Delta z} < C \tag{22}$$

where C is a constant which depends on the equation to be solved and not on the discrete parameters (i.e., Δt and Δx). C ranges between 1 and 7 depending on the velocity of wave propagation. In this study, C ranges from 1 to 3. The sum of the terms $u\Delta t/\Delta$ is defined as the Courant number. Before starting the calculation, *Hemera 1.0* analyses meteorological and oceanographic data in order to determine the possibility of convergence, depending on the magnitudes of the resultant velocities over the entire temporal domain.

Taking into account the air movement, the convection profile depends on the vertical distribution of the wind speed (u(z)), given by [33]

$$u(z) = u_{ref} \left(\frac{z}{z_{ref} - z_0} \right)^{1/7} \tag{23}$$

where u_{ref} is the wind speed at a given height z. The wind distribution in x and y components is given by the wind direction over the local terrain.

2.3. BOUNDARY CONDITIONS

The surface energy balance seems to be a reasonable method to establish the surface temperature boundary conditions, because it tends to preserve the cause-effect relationship between surface temperatures and heat fluxes. As mentioned before, the model solves 3D heat diffusion equations in combination with bulk aerodynamic formulas [44]. This allows the quantification of physical phenomena such as the heating of sediment/water temperature as a result of exposure to solar radiation. In addition, it is possible to evaluate changes in system conditions such as thermal diffusivity of sediment, water or air and changes in surface reflection (α).

The equation (24) is used as surface boundary condition to quantify thermal variations, where the advective heat flux is considered equal to zero [25, 27]

$$\lambda_{QG} \left. \frac{\partial T}{\partial z} \right|_{z=Z\,\sup} = Q_H + K\downarrow(1-\alpha) + L\downarrow - L\uparrow - L_E \tag{24}$$

where λ_{QG} is the thermal conductivity [W m^{-1} K^{-1}] of the element in question, Q_H is the sensible heat flux, K and L are the short and long wave radiation, respectively, and L_E is the latent heat flux. By substitution of the equivalent terms in equation (24) and by using an analytical approach, we obtain the following surface boundary condition, which is determined by the value of its respective thermal gradient

$$\left. \frac{\partial T}{\partial z} \right|_{z=Z\,\sup} = \frac{Q_H + R_N\left(1-\frac{\Delta}{\Theta}\right) - \beta}{\lambda_{QG}\left(1+\frac{\Delta}{\Theta}\right)} \tag{25}$$

$$\Theta = \Delta + \gamma\left(1+\frac{r_s}{r_a}\right) \tag{26}$$

$$\beta = \frac{\rho cp\left(e_s - e_a\right)}{r_a \Theta} \tag{27}$$

where R_N is the net radiation.

The value of the derivative (Eq.18) of surface boundary condition (Eq. 25) is replaced by the nodes of the sediment/water surface. Using the boundary condition in equation (25), the atmosphere and sediment/water surfaces are coupled, giving stability to the model. Besides, this makes it possible to analyze most of the physical phenomena related to the heat balance according to the environmental conditions. These equations, in combination with energy balance equations, allow us to describe and model the thermal behaviour of complex environments in an iterative and intelligent system like *Hemera 1.0*.

2.4. SOFTWARE DESCRIPTION

Hemera 1.0 is a software tool developed for modeling the heat exchange, especially applicable to environments that integrate the coupled sediment-water-atmosphere surface. A 3D finite-difference solution was implemented using object oriented programming in *Delphi 6.0* and an open-source philosophy (Appendix Fig. 1). The software integrates several mathematical models and has a graphical interface for managing of pre- and post-processing data. *Hemera 1.0* simulates physical processes in the water column, as well as in the sediments and air; besides, it is able to simulate the coupling between these surfaces. Each of the parameters involved in the model are fully user-configurable through text files, which have a basic structure.

The interface is comprised of two main functional areas (Fig. 2): geovisualization and command line (CLI). *OpenGL* was used to render the results. *Hemera 1.0* generates a dynamic 3D visualization of the terrain from a digital elevation model (DEM). DEM (or bathymetry) data in existing files are incorporated within the calculation procedure. The software allows users to perform view control (e.g., zoom, view angles, view position), light position control, screen selection, etc. To represent terrain variables, several visual metaphors

were used [e.g., 22, 28]; this enables a wide visualization of the terrain and its interaction with the tide. The CLI has interactions with a computer system and allows perform specific tasks through specific written instructions. A command interpreter designed for *Hemera 1.0* receives, analyzes and executes the requested command.

Hemera 1.0 generates multiple visual and numerical outputs (Fig. 2) which are stored in the same directory. A significant amount of data is generated, which is divided into multiple files. In this sense, the software also allows users to select points, profiles and areas individually for further analysis, where each output is saved in a separate file from the master files. This procedure has the advantage of studying the behaviour of given sectors of the study area, without using all the available information.

The model was implemented in four main threads concerning the manipulation of the user interface, geovisualization, modeling and writing files. The numerical calculation of each step (Δt) is transferred to multiple tasks in parallel (up to 128). Therefore, this implementation allows *Hemera 1.0* to maximize the computing capacity of a system as well as to minimize memory consumption. Because each node (discrete point) depends only on the previous step, this enables to carry out multiple computing processes at the same time, with no dependency between them. It is also possible to work with partial sections within a grid (i.e., digital terrain) to minimize memory consumption. This process is important when a study area involves a significant size.

Physical variables (e.g., air, sediment or water temperature, among others) are read from the file, to be subsequently used in successive iterations. An iterative sequence let the user to carry out determinations of the spatial and temporal temperature, whenever stability conditions are fulfilled. Figure 3 shows a flowchart of the iteration with its respective alternations. The system iterates a set of equations (e.g., equations 23, 21, 25) until the total simulation time is reached or until the defined criterion for convergence is fulfilled. If the average surface temperature variation ($|T_s|$) between steps is less than a boundary value (δ) (i.e., $|T_s|<\delta$) this will be considered as convergence condition.

To achieve the effective value of the system, the procedure involves many iterations (Fig. 3). Certain processes, such as the complexity of the system (Eq. 21), the surface resolution temperature, as well as the number of iterations, prove the advantages of using the explicit Euler method on parallel, to facilitate the implementation and to achieve high convergence rates with minimal memory consumption.

There are basic files used to configure the model: the *general parameter* file, in which file names, grid DEM, meteorological and oceanographic data, output folder, among others, are defined; also the input file of *meteorology* and *oceanography*, containing records sorted by Julian date of variables such as air temperature, relative humidity, atmospheric pressure, wind, tides, waves (height and period) and suspended sediments. The data input of the two latter variables are optional because they can be estimated by the model. The *geovisualization* file is focused on the definition of the elements for rendering a terrain such as lighting, transparency, reflections, among others (Fig.2a). Finally, the *energy balance* file, in which coefficients for the calculation of R_N, parameters for estimating α in sediment and water, height values of terrain, among others, are defined.

Specific files were defined focused on measurements on particular sectors of the terrain such as, vertical and longitudinal profiles. These files, termed Distributed Temperature Sensing (DTS), enable users to configure *Hemera 1.0* in order to store simulation results of specific nodes in a separate file.

3. RESULTS AND DISCUSSION

3.1. DESCRIPTION OF STUDY AREA AND ACQUIRED DATA

The selected area to carry out the simulation is SVM, located in a temperate climate zone. The estuary comprises an area of 2,300 km^2 and it is classified as a mesotidal coastal plain. The mechanical energy input into the system is produced by a semidiurnal tidal wave [31]. The average tidal range increases from the mouth (2.2 m) to the estuary head (3.5 m) [32]. The mean spring and neap tide ranges between 2.7 and 1.8 m at the mouth, respectively, while at the head they ranges between 4 and 3 m [32]. The estuary constitutes an ecological system under a humid temperate climate, covered largely by vascular vegetation (e.g., *Spartina alterniflora* and *Sarcocornia perennis*). Sediments granulometry indicates the predominance of a silty sand texture [44].

In order to demonstrate the effectiveness of the model, we have selected the month of January because in this month the thermal and radiative energy show the highest fluctuations [44]. The measured parameters are shown in figure 5. Solar radiation showed a typical behaviour, with average maximum values of 950 Wm^{-2} (Fig. 5a). The daily air temperature amplitude showed an average of 16.4°C, with a maximum of 22.2°C (Fig. 5b). The average wind speed reached values of 6.6 m s^{-1}, with periods of calm of less than 3 hours, while the maximum speed reached 23.4 m s^{-1} (Fig. 5d).

3.1.1. DIGITAL ELEVATION MODEL

A DEM was generated using a geoprocessing technique, applied to images taken on the intertidal zone of the SVM (Fig. 6). It is assumed that the tide line constitutes a line of equal elevation, thus it is possible to generate a DEM using tide lines at different stages. Two digital cameras were installed (10 megapixels), which were located in specific sites to cover a significant portion of the area to be modeled. The cameras were connected to an intelligent shutter release which was pressed down thrice at an interval of 10 minutes.

For each set of three images, an average image was obtained for evening out short variations due to wind and other perturbations. Subsequently, the sequence of images was integrated into a Geographic Information System (GIS) in order to digitize tide lines (Fig. 6). To generate the altimetric value for each line, the height of the tide was simultaneously recorded. The digitized lines were transferred to a flat space through the application of the planar projective transformation (WGS 84). A grid was obtained through interpolation using standard software. Three types of grids (terrain) were generated at low, medium and high resolution, corresponding to the following 3D grid spacing xyz: 3x3x0.5, 1x1x0.1 and 0.5x0.5x0.05 m, respectively. Finally, these grids are exported to **.grd* format, to be imported in *Hemera 1.0*.

3.2. OPERATIONAL IMPLEMENTATION

The results were obtained using the higher spatial resolution data (grid spacing= 0.5x0.5x0.05 m) with a total size of 440x220x8.5 m. According to the physical space and the spatial discretization, the model has 65,824,000 nodes. The zero level of the tide gauge was taken as a reference plane (Z=0) in the DEM. The upper reference plane is given by $T_Z=5.5=T_{air}$. Finally, in the lower reference plane (Z=-3m) a constant value of 16.5ºC (i.e., T_Z=-3m=16.5ºC) was considered.

An uniform vegetal cover was considered in order to simplify the surface configuration of the model. In addition, the water and sediment reflection coefficient for January is 0.095 and 0.111, respectively [44].

The location of the DTSs on the virtual terrain is shown in figure 7. The DTS0 is located in the upper sector which is occasionally flooded. The DTS1 is located at the site of the temperature measurements at different depths (0.05, 0.15 and 0.30 m). The DTS2 is located in the lower sector which is flooded during more than 50% of the time (i.e., 56 %). Finally, the DTS3 is located in a sector which is flooded during more than 90% of the time.

3.3. MODEL VALIDATION

A comparative analysis of the model results with direct field measurements was carried out to validate the model using *Hemera 1.0*. The comparison was made at 0.15 m depth, in response to significant fluctuations of temperature at shallow depths (Fig. 8). As a result, the simulated time series showed an average of 22.5°C; therefore, the difference with the measured average temperature (DTS1: 21.9°C) was 0.6°C (Fig. 8). The simulated time series shows sufficient stability over time. It evolves from its initial condition (day 1, 19°C) and becomes stabilized after the first 2 days.

The simulated time series showed an average relative error of 3.3% during the study period. The error showed a cyclical evolution. The average time of stabilization (error<3.3%) takes 2 days and 6 hours (Fig. 9a). Once stabilized, the error values are lower than 5%, where the model is able to keep temporal stability, showing a correct performance. Other periods in which the maximum error occurs, were analyzed in great detail (Figs. 9b-9e). Because the inherent variation in the boundary conditions (e.g., tide, wind or air temperature) the simulation moves away from the measured value, but keep adequate stability with a maximum error of 12.7%. Therefore, the numerical simulation in a real system provides reliable high performance, regardless of the behaviour of the boundary conditions.

3.4. RESULTS OF SIMULATION

The results of the simulation over the whole study area in January 2009 showed an average surface sediment temperature of 24.4°C, with a minimum value of 18.2ºC and a maximum of 33.3ºC. In the case of the water temperature (tide height>0.5 m), its average value was 22.1°C, with a minimum value of 19.6°C and a maximum of 26.4ºC.

Vertical profiles of sediment temperature (from 0 to 0.3 m layer) and of air/water temperature (from 0 to 2 m layer) were obtained for the selected study sites (Fig. 10). In general terms, the largest magnitudes of vertical temperature gradient, usually $T_{air}<T_{sediment}$, occur in the upper sector of the saltmarsh (Fig. 10). It should be noted that the intertidal sediment temperature shows fluctuations over time which are caused by the immersion-emersion alternation combined with the solar cycle [15].When the sediments are exposed to the atmosphere at low water, the heat penetrates into the sediment layer mainly up 0.10-0.25 m depth in the sites DTS1 and DTS2 (Figs. 10b and 10c), while in the remaining sector the heat reaches deeper soil levels (Fig. 10a). This particularity can be attributed to the presence of a relatively deep zone of aeration in the upper sector.

Thermal effects of the flood tide on the first layer of sediment and air can be clearly observed in the temperature profiles. It takes place over very brief period and reduces the steepness of the temperature gradient. In general, the surface sediment temperature showed a considerable decrease (about 1 to 3°C) during the flood tide. Below this surface layer,

temperature decreases gradually up to some hours after the end of flood tide, when it begins to show an inverted temperature profile. At other times, during immersion period, the bottom water temperature is slightly warmer than in the rest of the water column.

Tidal inundation also influences the thermal regime of the study area. The highest temperatures occurred in the upper sector, where the flood tide period is occasional (Figs. 10 and 11). The amplitude of surface sediment temperature was also greater in the upper (ΔT_{max}=20.7ºC) than in the lower sector (ΔT_{max}=15ºC). The attenuation effects of the tide in the latter sector can be clearly seen (Fig. 11). The sites DTS1 and DTS2 showed a similar thermal behaviour (Figs. 10b and 10c). On the other hand, it is notable that both sediment and water temperature during the first 10 days were mostly temperate than in the remaining period.

3.5. PREDICTIVE ANALISYS

In order to arrive at different predictions of the thermal interactions of the system, a series of simulations were carried out considering, on one hand, different boundary conditions related to meteorological parameters and, on the other hand, variations in the vegetation cover (Figs. 12 and 13). Two boundary conditions were arbitrary selected: a) an increase in air temperature of 30%; b) an increase in wind speed of 30%. In the case of vegetation cover, a soil without vascular vegetation, with a surface resistance of zero (rs=0) was selected.

Figure 12 shows the evolution of the sediment temperature at 0.15 m depth for the three study sites, including the simulated time series and the field measurements. The average sediment temperature corresponding to the measured time series was 23.2°C. The simulations demonstrate that the sediment temperature increased significantly due to increasing air temperature. By varying the air temperature, the average sediment temperature was 26.1°C. Particularly, this increase occurred strongly in the upper sector (occasionally flooded) with an average increase of 19.3% (Fig. 12a). The remaining sites (i.e., DTS1 and DTS2) showed an average increase of 9.3 and 7.7%, respectively. By varying the wind speed, the average sediment temperature was 23.3°C; therefore, its influence on sediment temperature was generally very low or null. In the lower sector can be observed an average increase in sediment temperature of 0.7 and 0.8%, respectively (Figs. 12b and 12c), while in the upper sector it resulted in a decrease of 0.8% (Fig. 12a). The lack of vegetation generated an average sediment temperature of 23°C. This condition produced a slight decrease in sediment temperature of only 1.2, 0.7 and 0.6% for the sites DTS0, DTS1 and DTS2, respectively (Fig. 12).

The modeled surface temperature along the study area showed variations (Fig. 13). With an increase in air temperature of 30%, the average sediment temperature increased from 24.4 to 29.6°C (i.e., 21.3%), while the average water temperature increased from 24.3 to 26.5°C (i.e., 9%). But, like the previous results presented in figure 12, the increase of wind speed and the lack of vegetation cover, both had a low influence on the surface temperature (sediment/water) compared to the increase of the air temperature, of the order of 1 to 4%. For instance, the increase of wind speed produced an increase in average temperature of sediment and water of 3.7 and 1.8%, respectively. Despite this low effect on the thermal interactions, the wind speed (+30%) produced an increase of sensible heat flux that caused a decrease of sediment temperature during the night hours. The lack of vegetation produced an increased of average temperature of sediment and water of 2.5 and 1.4%, respectively.

These results show that a change in air temperature produces a significant variation in the surface temperature, being higher in the high sector of the SVM, where the resident time

of water is low (Figs. 12b and 13b). In this sense, during the simulated period, the surface sediment temperature had an oscillation range of 23.3°C (19.9 to 43.2°C), 18.1°C (17.8 to 35.9°C) and 16.5°C (18.2 to 34.7ºC), according to the variation of the air temperature, the wind speed and the vegetation cover, respectively. The surface water temperature exhibited smaller thermal amplitude than the sediment temperature, 10.3°C (20.1 to 30.4°C), 8.5°C (19.4 to 28.1°C) and 7.8°C (19.6 to 27.4ºC), according to the variation of the air temperature, the wind speed and the vegetation cover, respectively.

4. CONCLUSIONS

This work described a 3D numerical model through the employment of finite-difference approximation for the simulation, prediction and visualization of sediment, water and air temperature, applied in the Villa del Mar saltmarsh, Bahía Blanca Estuary (Argentina) in January 2009. In order to carry out this computation, an open-source software *Hemera 1.0* was developed.

Generally, the simulated time series adequately describes the daily cycles, showing high concordance with the field measurements. As a result of validating the model with measured data at 0.15 m depth, where thermal fluctuations are strong, the simulated time series presented an average relative error of 3.3% and a maximum relative error of 12.7%. The error showed a cyclical behaviour, in which the average time of stabilization (i.e., error<3.3%) takes 2 days and 6 hours.

According to the modeling results, the maximum temperatures occurred in the high sector of the saltmarsh, where the flood tide is occasional. The amplitude of surface sediment temperature was also greater in the upper (ΔT_{max}=20.7ºC) than in the lower sector (ΔT_{max}=15ºC), in response to attenuation effect of the tide. The temperature profiles showed a clearly effect of the flood tide on the first layer of sediment and air. Every day showed a considerable decrease (about 1 to 3°C) in surface sediment temperature during the flood tide.

The model showed an adequate response to changes in the boundary conditions and in the vegetation cover and it reproduces adequately the physical processes of the heat balance in coastal areas. The air temperature is the most important parameter in both surface and depth (0.15 m) temperature behaviour, particularly when the time of exposure to the atmosphere is greater, agreeing with the measurements made on SVM. In contrast, the increase of wind speed and the lack of vegetation both had a very low influence on temperature. In the case of wind speed, the strong winds produce a significant decrease in the surface temperature of the sediment at night.

Hemera 1.0 is characterized by having little complexity and low hardware requirements. In addition, it has the advantage that requires few data input such as meteorological and oceanographic variables and some soil properties. *Hemera 1.0* provides reliable high performance, regardless of the boundary conditions behaviour. It is easily adaptable to other environments such us lakes, lagoons, reservoirs, among others, in order to carry out similar studies.

REFERENCES

1. Bateni, S. M., Jeng, D. S. & Mortazavi Naeini, S. M. (2012). Estimating soil thermal properties from sequences of land surface temperature using hybrid Genetic Algorithm–Finite Difference method. *Engineering Applications of Artificial Intelligence*, 25(7), 1425-1436.

2. Befus, K. M., Bayani Cardenas, M., Erler, D. V., Santos, I. R., Eyre, B. D. (2013). Heat transport dynamics at a sandy intertidal zone. *Water Resources Research*. DOI:10.1002/wrcr.20325
3. Beigt, D., Piccolo, M. C. & Perillo, G. M. E. (2008). Surface heat exchanges in an estuarine tidal flat (Bahía Blanca Estuary, Argentina). *Ciencias Marinas*, 34(1), 1-15.
4. Beletsky, D. & Schwab, D. J. (2001). Modeling circulation and thermal structure in Lake Michigan: Annual cycle and interannual variability. *Journal of Geophysical Research*, 106(C9), 19,745-19,771.
5. Blyth, E. M., Dolman, A. J. & Wood, N. (1993). Effective resistance to sensible- and latent-heat flux in heterogeneous terrain. *Quart. J. Roy. Meteor. Soc*., 119, 423-442.
6. Courant, R., Friedrichs, K. & Lewy, H. (1967). On the partial difference equations of mathematical physics (English translation of the 1928). *IBM Journal*, 215-234.
7. de Szoeke, S. P., Fairall, C. W., Wolfe, D. E., Bariteau, L. & Zuidema, P. (2010). Surface Flux Observations on the Southeastern Tropical Pacific Ocean and Attribution of SST Errors in Coupled Ocean–Atmosphere Models. *Journal of Climate*, 23(15), 4152-4174.
8. Fang, X. & Stefan, H. G. (1997). Temperature variability in lake sediments. *Water Resources Research*, 34(4), 717-729.
9. Ferreira, D. & Marshall, J. (2010). The role of the hydrological cycle in coupled atmosphere-ocean heat transport. Proceedings from the *AGU 2010 Ocean Sciences Meeting*, 22-26 Feb.
10. Genova, S. N., Belolipetskii, V. M., Rogozin, D. Y., Degermendzhy, A. G. & Mooij, W. M. (2010). A one-dimensional model of vertical stratification of Lake Shira focussed on winter conditions and ice cover. *Aquat Ecol.*, 44, 571-584.
11. Golosov, S. & Ignatieva, N. (1999). Hydrothermodynamic features of mass exchange across the sediment–water interface in shallow lakes. *Hydrobiologia*, 408-409, 153-157.
12. Golosov, S. & Kirillin, G. (2010). A parameterized model of heat storage by lake sediments. *Environmental Modelling & Software*, 25(6), 793-801.
13. Goyette, S. & Perroud, M. (2012). Interfacing a one-dimensional lake model with a single-column atmospheric model: Application to the deep Lake Geneva, Switzerland. *Water Resources Research*, doi:10.1029/2011WR011223.
14. Gu, R. & Stefan, H. G., 1990. Year-round temperature simulation of cold climate lakes. *Cold Regions Science and Technology*, 18(2), 147-160.
15. Guarini, J. M., Blanchard, G. F., Gros, P. & Harrison S. J. (1997). Modelling the mud surface temperature on intertidal flats to investigate the spatio-temporal dynamics of the benthic microalgal photosynthetic capacity. *Mar. Ecol. Prog. Ser.*, 153, 25-36.
16. Han, B., Armengol, J., Garcia, J. C., Comerma, M., Roura, M., Dolz, J. & Straskraba, M. (2000). The thermal structure of Sau Reservoir (NE: Spain): a simulation approach. *Ecological Modelling*, 125(2-3), 109-122.
17. Harrison, S. J. & Phizacklea, A. P. (1985). Seasonal changes in heat flux and heat storage in the intertidal mudflats of the Forth Estuary, Scotland. *Journal of Climatology*, 5, 473-485.
18. Harrison, S. J. & Phizacklea, A. P. (1987). Temperature fluctuation in muddy intertidal sediments, Forth estuary, Scotland. *Estuar Coast Shelf Sci*, 24, 279-288.
19. Hebert, C., Caissie, D., Satish, M. G. & El-Jabi, N. (2011). Study of stream temperature dynamics and corresponding heat fluxes within Miramichi River catchments (New Brunswick, Canada). *Hydrol. Process.*, 25, 2439-2455.
20. Incropera, F. & De Witt, D., 1990. *Fundamentals of Heat and Mass Transfer*. 3rd.ed., John Wiley & Sons.
21. Jafarov, E. E., Marchenko, S. S. & Romanovsky, V. E. (2012). Numerical modeling of permafrost dynamics in Alaska using a high spatial resolution dataset. *The Cryosphere Discussions*, 6, 89-124.
22. Kilgard, M. (1996). *OpenGL for the X Window System*. Addison-Wesley.
23. Kim, T. W., Cho, Y. K. & Dever, E. P. (2007). An evaluation of the thermal properties and albedo of a macrotidal flat. *Journal of Geophysical Research: Oceans*, 112, 1-9.
24. Kim, T. W. & Cho, Y. K. (2011). Calculation of heat flux in a macrotidal flat using FVCOM. *Journal of Geophysical Research: Oceans*, 116, 2156-2202.

25. Krarti, M., Lopez-Alonzo, C., Claridge, D. E. & Kreider, J. F., 1995. Analytical model to predict annual soil surface temperature variation. *Solar Energy Eng.*, 117(2), 91-99.
26. Mihalakakou, G., Santamouris, M., Lewis, J. O. & Asimakopoulos, D.N. (1997). On The Application Of The Energy Balance Equation To Predict Ground Temperature Profiles. *Solar Energy*, 60(3/4), 181-190.
27. Mihalakakou, G. (2002). On estimating soil surface temperature profiles. *Energy Buildings*, 34, 251-259.
28. Lengyel, E. (2003). *The OpenGL Extensions Guide*. Charles River Media.
29. Micheels, A., Bruch, A. A., Eronen, J., Fortelius, M., Harzhauser, M., Utescher, T. & Mosbrugger V. (2011). Analysis of heat transport mechanisms from a Late Miocene model experiment with a fully-coupled atmosphere–ocean general circulation model. *Palaeogeography, Palaeoclimatology, Palaeoecology*, 304(3-4), 337-350.
30. Na, J. S., You, S. & Seo, J. (2000). Seasonal variation of the heat flux in muddy intertidal sediments near the Jebu Island during the ebb tides in the west coast of Korea. *Journal of Korean Society of Oceanography*, 5, 1-9.
31. Perillo, G. M. E., Parodi, E. & Freije, R. H. (2001). *The Bahia Blanca Estuary, Argentina*. In U. Seeliger & B. Kjerfve (Eds.), Coastal Marine Ecosystems of Latin America (pp. 205-217). Springer Berlin Heidelberg.
32. Perillo, G. M. E, Piccolo, M. C., Palma, E. D., Pérez, D. E. & Pierini, J. O. (2004). *Oceanografía Física*. In M. C. Piccolo & M. Hoffmeyer (Eds.), Ecosistema del estuario de Bahía Blanca (pp. 61-67). Editorial Sapienza, Argentina.
33. Peterson, E. W. & Hennessey, J. P.(Jr) (1978). On the use of power laws for estimates of wind power potencial. *J. Appl. Meteorology*, 17, 390-394.
34. Piccolo, M. C. & Pierini, J. (1986). Numerical simulation of a stable planetary boundary layer over the argentine continental shelf. *Boundary-layer Meteorology*, 37, 229-243.
35. Piccolo, M. C., Perillo, G. M. E. & Daborn, G. R. (1993). Soil temperature variations on a tidal flat in Minas Basin, Bay of Fundy, Canada. *Estuarine & Coastal Shelf Science*, 35, 345-357.
36. Press, W. H., Flannery, B. P., Teukolsky, S. A. & Vetterling, W. T. 1992. *Numerical Recipes in FORTRAN: The Art of Scientific Computing.* 2nd ed., Cambridge University Press, Cambridge, England.
37. Rotunno, R. & Emanuel, K. A. (1987). An air–sea interaction theory for tropical cyclones. Part II: Evolutionary study using a nonhydrostatic axisymmetric numerical model. *J. Atmos. Sci.*, 44, 542-561.
38. Sequeira, M. E. & Piccolo, M. C. (1985). Predicción de la temperatura del agua durante la bajante de la marea en Ingeniero White. *Meteorológica*, 15(1), 59-76.
39. Silliman, S. E., Ramirez, J. & McCabe, R. L. (1995). Quantifying downflow through creek sediments using temperature time series: one-dimensional solution incorporating measured surface temperature. *Journal of Hydrology*, 167(1–4), 99-119.
40. Stathers, R. J., Black, T. A. & Novak, M. D., 1988. Modelling surface energy fluxes and temperature in a dry and wet bare soils. *Atmosphere-Ocean*, 26(1), 59-73.
41. Tianjun, Z., Rucong, Y. & Zhaoxin, L. (2002). ENSO-dependent and ENSO-independent variability over the mid-latitude North Pacific: Observation and air-sea coupled model simulation. *Advances in Atmospheric Sciences*, 19(6), 1127-1147.
42. Thomson, J. (2010). Observations of thermal diffusivity and a relation to the porosity of tidal flat sediments. *Journal of Geophysical Research*, 115, 1-6.
43. Tsay, B. T. K., Ruggaber, G. J., Effler, S. W. & Driscoll, C. T. (1992). Thermal stratification modeling of lakes with sediment heat flux. *J. Hydraul. Eng.*, 118(3), 407-419.
44. Vitale, A. J. (2010). *Modelado y simulación del balance energético en marismas*. Doctoral Thesis, Universidad Nacional del Sur, Argentina.

FIGURE CAPTIONS

Fig. 1 Finite-difference code implementation for the threads, according to its respective rank assigned (i_ini to i_fin) **(Appendix)**
Fig. 2 Renderized 3D view of the study area (a) and the multiline command window in *Hemera 1.0* (b)
Fig. 3 Flowchart diagram showing sequential iteration with *Hemera 1.0* (Appendix Fig.4)
Fig. 4 Extract of the main thread code implementation, oriented to main iteration control to solve the modeling **(Appendix)**
Fig. 5 Meteorological and oceanographic variables measured in January 2009(Day 0=01/01/2009). Solar radiation (a), air temperature (b), relative humidity (c), wind speed (d) and tide level (e)
Fig. 6 Example of the elevation contour lines within the field of vision area of a camera mapped using a GIS, in the SMV. Digitized contour lines without transformation to the flat space (a) and with transformation to the flat space (b)
Fig. 7 Location of the DTSs on the virtual terrain and the sign convention for the axes. The upper sector is occasionally flooded while the lower sector is periodically flooded
Fig. 8 Measured and simulated sediment temperature time series at a depth of 0.15 m in the site of measurement (DTS1)
Fig. 9 Relative error expressed in absolute terms of the sediment temperature at 0.15 m depth in the site DTS1, for 31 days (a), from day 1 to day 4 (b), from day 5 to day 9 (c), from day 11 to day 15 (d) and from day 19 to day 23 (e)
Fig. 10 Temperature profiles modeled for the different sectors, from day 1 to day 29. Profile in sector DTS0 (a), profile in sector DTS1 (b), profile in sector DTS2 (c) and tide level (d)
Fig. 11 Surface temperature modeled along a profile crossing the intertidal area using DTS3 and its comparison with the tide level at the site from day 1 to day 14 (a) and from day 15 to day 29 (b)
Fig. 12 Sediment temperature time series at a depth of 0.15 m considering the different boundary conditions, the variation in the vegetation cover and the measured data for the study sites in January 2009. Location DTS0 (a), location DTS1(b) and location DTS2 (c)
Fig. 13 Simulated surface temperature along the study area from day 1 to day 29, considering the different boundary conditions, the variation in the vegetation cover and the measured data. Measured data (a), air temperature (+30%) (b), wind speed (+30%) (c), without vegetation cover (rs=0) (d) and tide level (e)

Click here to download high resolution image

```
////////////////////////////////////////////////////////////////////////////////
procedure TEulerHeat3D.ModelarEstadoSigThreads(Sender: TObject);
var
  i,j,k, kw         : word;
  pG2DK             : pGrilla2DK;  // Pointer to discrete surface
  pG3D_N            : pGrilla3D;   // Pointer to actual 3D terrain Grid
  pG3D_N1           : pGrilla3D;   // Pointer to next 3D terrain Grid
  ks                : real;        // Thermal diffusivity of the node
  i_ini             : word;
  i_fin             : word;
  T                 : real;        // Temperature of the node

  ddxtt, ddytt, ddztt : real;      // Second derivatives of T
  ddxt, ddyt, ddzt    : real;      // First derivatives of T
  ddxk, ddyk, ddzk    : real;      // First derivatives of thermal diffusivity
  vx, vy, vz          : real;      // Speed component

begin

  // Configure procesing range
  i_ini := (Sender as TRangoGrilla).getValueInicial;
  i_fin := (Sender as TRangoGrilla).getValueFinal;

  // Assign the pointers to the 2D and 3D grids
  pG2DK   := GrillaN.GetPunteroG2DK;
  pG3D_N  := GrillaN.GetPunteroG3D;
  pG3D_N1 := GrillaN1.GetPunteroG3D;
  kw      := GrillaN.getTidalLevelK;

  // Correct the range to contemplate the boundary
  if ((Sender as TRangoGrilla).getID = 0) then i_ini := 1;
  if ((Sender as TRangoGrilla).getID = nThreads-1) then i_fin := GrillaN.Numy-2;

  //----------------------------------------------------------------------------
  // Model the system for the next step upon the volume
  for k:= 1 to GrillaN.Numz-2 do begin
    for i:= 1 to GrillaN.Numx-2 do begin
      for j:= i_ini to i_fin do begin

        T   := pG3D_N^[i,j,k].T;
        ks  := pG3D_N^[i,j,k].dft;
        vx  := pG3D_N^[i,j,k].vx;
        vy  := pG3D_N^[i,j,k].vy;
        vz  := pG3D_N^[i,j,k].vz;

        // Discrete T (2Th) [m^2/s   °C/m^2 ]
        ddxtt := ( pG3D_N^[i+1,j,k].T - 2*pG3D_N^[i,j,k].T + pG3D_N^[i-1,j,k].T ) / ( dx*dx );
        ddytt := ( pG3D_N^[i,j+1,k].T - 2*pG3D_N^[i,j,k].T + pG3D_N^[i,j-1,k].T ) / ( dy*dy );
        ddztt := ( pG3D_N^[i,j,k+1].T - 2*pG3D_N^[i,j,k].T + pG3D_N^[i,j,k-1].T ) / ( dz*dz );

        // Discrete Ks [m^2/s   °C/m^2 ]
        ddxk  := ( pG3D_N^[i+1,j,k].dft - pG3D_N^[i-1,j,k].dft ) / ( 2*dx );
        ddyk  := ( pG3D_N^[i,j+1,k].dft - pG3D_N^[i,j-1,k].dft ) / ( 2*dy );
        ddzk  := ( pG3D_N^[i,j,k+1].dft - pG3D_N^[i,j,k-1].dft ) / ( 2*dz );

        // Discrete T
        ddxt  := ( pG3D_N^[i+1,j,k].T - pG3D_N^[i-1,j,k].T ) / ( 2*dx );
        ddyt  := ( pG3D_N^[i,j+1,k].T - pG3D_N^[i,j-1,k].T ) / ( 2*dy );
        ddzt  := ( pG3D_N^[i,j,k+1].T - pG3D_N^[i,j,k-1].T ) / ( 2*dz );

        // If the node corresponds to the surface water or sediment apply surface condicition
        if (k = pG2DK^[i,j]) or ( (k = kw) and (pG2DK^[i,j]<kw) ) then begin

          if (pG3D_N^[i+1,j,k].mEle <> pG3D_N^[i-1,j,k].mEle) and
             ( (pG3D_N^[i+1,j,k].mEle = meAire) or (pG3D_N^[i-1,j,k].mEle = meAire) ) then begin
            ddxtt := 0;
            ddxt  := 0;
          end;
```

Click here to download high resolution image

```
          if (pG3D_N^[i,j+1,k].mEle <> pG3D_N^[i,j-1,k].mEle) and
             ( (pG3D_N^[i,j+1,k].mEle = meAir) or (pG3D_N^[i,j-1,k].mEle = meAire) ) then begin
            ddytt := 0;
            ddyt  := 0;
          end;

          ddzt := SoilHeatFlux(i, j, k);
        end;

        // Open boundary condition
        // X => dt/dx = 0
        if (i=1) or (i=GrillaN.Numx-2) then begin ddxtt := 0; ddxt := 0; end;

        // Y => dt/dy = 0
        if (j=1) or (j=GrillaN.Numy-2) then begin ddytt := 0; ddyt := 0; end;

        // Calculate the temperature propagation
        pG3D_N1^[i,j,k].T := T + dt * ( ks * (ddxtt + ddytt + ddztt)
                                        + ddxk*ddxt + ddyk*ddyt + ddzk*ddzt
                                        - vx*ddxt   - vy*ddyt   - vz*ddzt
                                      );

      end;
    end;
  end;
  //---------------------------------------------------------------------------

  // Correct the range to contemplate the boundary
  if ((Sender as TRangoGrilla).getID = 0) then i_ini := 0;
  if ((Sender as TRangoGrilla).getID = nThreads-1) then i_fin := GrillaN.Numy-1;

  // Vertical boundary (closed)
  // Closed boundary condition Tx = T
  for i:= 0 to GrillaN.Numx-1 do begin
    for j:= i_ini to i_fin do begin
      pG3D_N1^[i,j,0].T              := tinf;
      pG3D_N1^[i,j,GrillaN.Numz-1].T := tsup;
    end;
  end;

  // Evaluate the change of the surface between the steps D = T(N) - T(N+1)
 (Sender as TRangoGrilla).setDifMaxRango( GrillaN.CalcularMaxDifSuperficie(GrillaN1, i_ini, i_fin) );

  // Evaluate the relative change of the surface between the steps D = T(N) - T(N+1)
 (Sender as TRangoGrilla).setDifRelRango( GrillaN.CalcularDifRelSuperficie(GrillaN1, i_ini, i_fin) );

  // Calculate the average surface temperature in T(N+1)
 (Sender as TRangoGrilla).setTMedSupRango( GrillaN.CalcularTMedSuperficie(GrillaN1, i_ini, i_fin) );

  // Calculate the average water surface temperature T(N+1)
 (Sender as TRangoGrilla).setTMedSupAgRango( GrillaN.CalcularTMedSuperficieAgua(GrillaN1, i_ini, i_fin) );

  // Reassign the resulted grid to the actual grid
  GrillaN.AsignarParteGrilla(GrillaN1, i_ini, i_fin);

  // Save the resulted grid into the disc
  GrillaN.GuardarGrilla3D(PathGrilla3D);
end;

////////////////////////////////////////////////////////////////////////////////
```

colour figure-2
Click here to download high resolution image

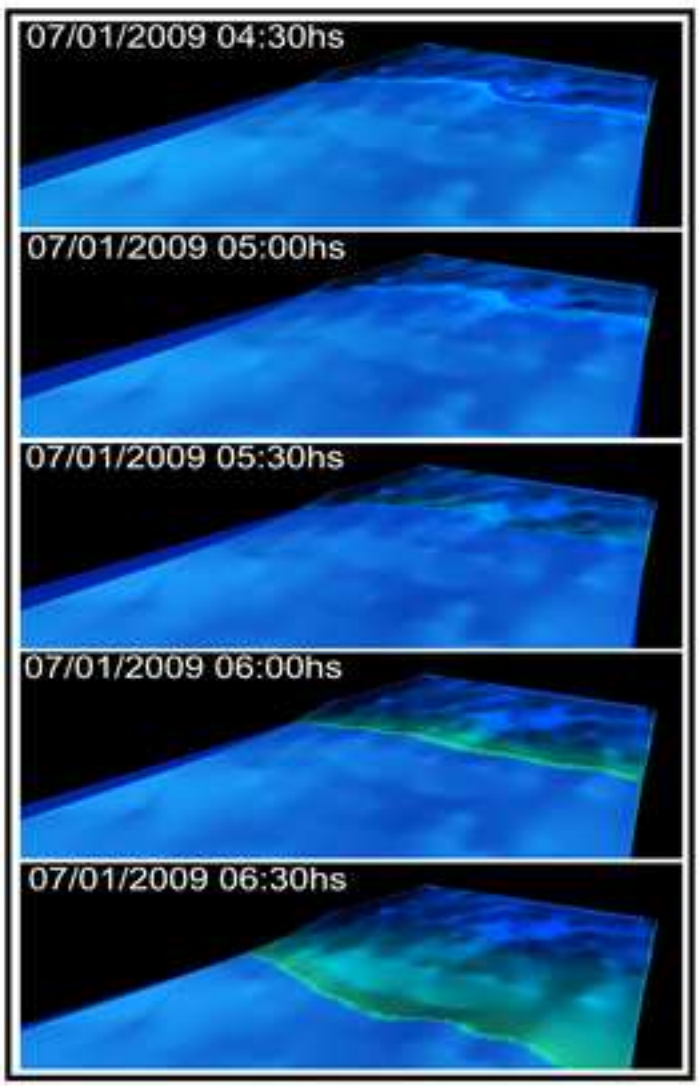

(a)

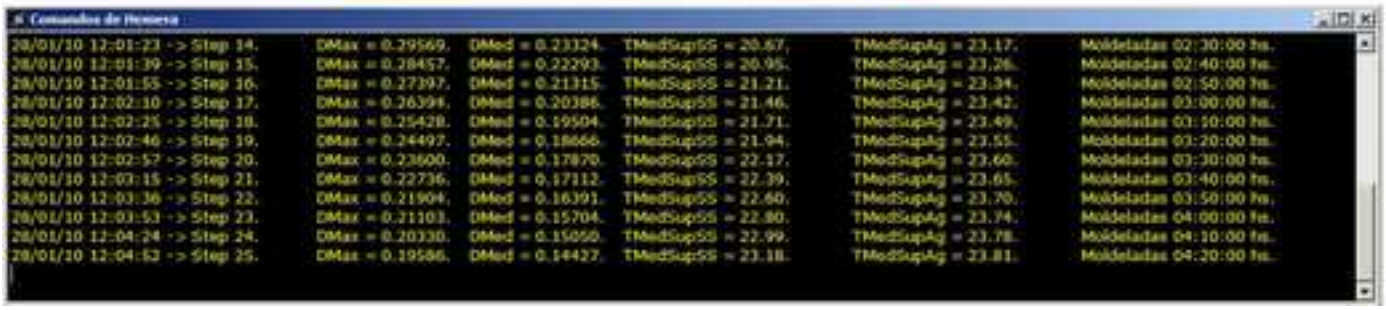

(b)

line figure-3
Click here to download high resolution image

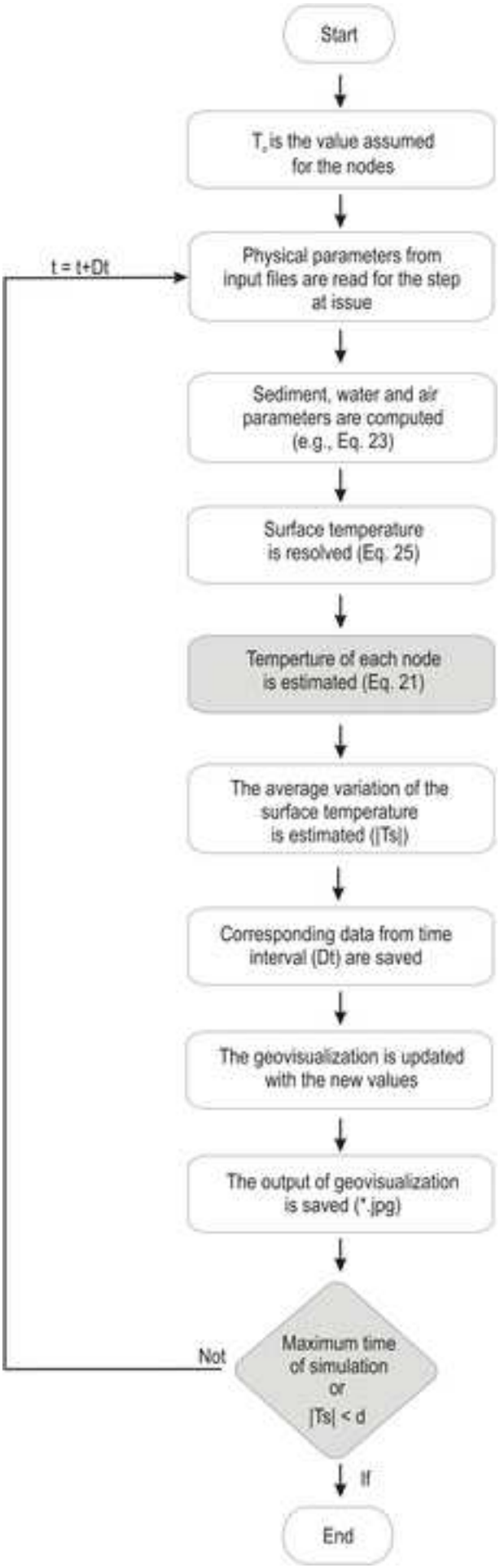

colour figure-4 (Appendix)
Click here to download high resolution image

```
...
while ( (Tpo < Tpof) and (DifSupMed > 0.005) ) do begin

  // Model the step on parallel
  ExecuteThreads;

  // Wait 100 ms for finish all threads
  while not allThreadsFinish do begin Retardo(100) end;

  // Obtain the variation in the surface temperature between steps of the threads
  DifSupMax := getDifMaxGrilla();
  DifSupMed := getDifRelGrilla();
  TMedSup   := getTMedSupGrilla();
  TMedSupAg := getTMedSupAgGrilla();

  // Update the surface in order to change the color according to the temperature
  Terreno.UpdateSurface;
  Agua.UpdateSurface;

  // Save a snapshot of the simulation into the disc
  SaveEsceneNow := true;

  // Save the DTS information
  SaveAllDTS;

  // Increase the step
  Tpo := Tpo + dt/86400;
  inc(nSteps, 1);

  // Obtain the data for the next simulation step
  getMeteoDataOfStep(Tpo);

  // Initialize the tide level
  GrillaN.setTidalLevel(TLev);
  Agua.setTidalLevel(TLev, GrillaN.getTidalLevelk() );

  // Reinitialize the water and air temperature
  SetupTempWaterNewTidal();

    end;
   end;
 end;

 // Update the surface in order to change the color according to the temperature
 Terreno.UpdateSurface;
 Agua.UpdateSurface;

 // Save a snapshot of the simulation into the disc
 SaveEsceneNow := true;

 // Message to LOG
 maje0 := 'Simulación términada. Liberando memoria.' ;

 // Wait for redraw the final scene
 Retardo(5000);

 // Destroy object
 EulerHeat3D.destruir;
end;

////////////////////////////////////////////////////////////////////////////////
```

line figure-5
Click here to download high resolution image

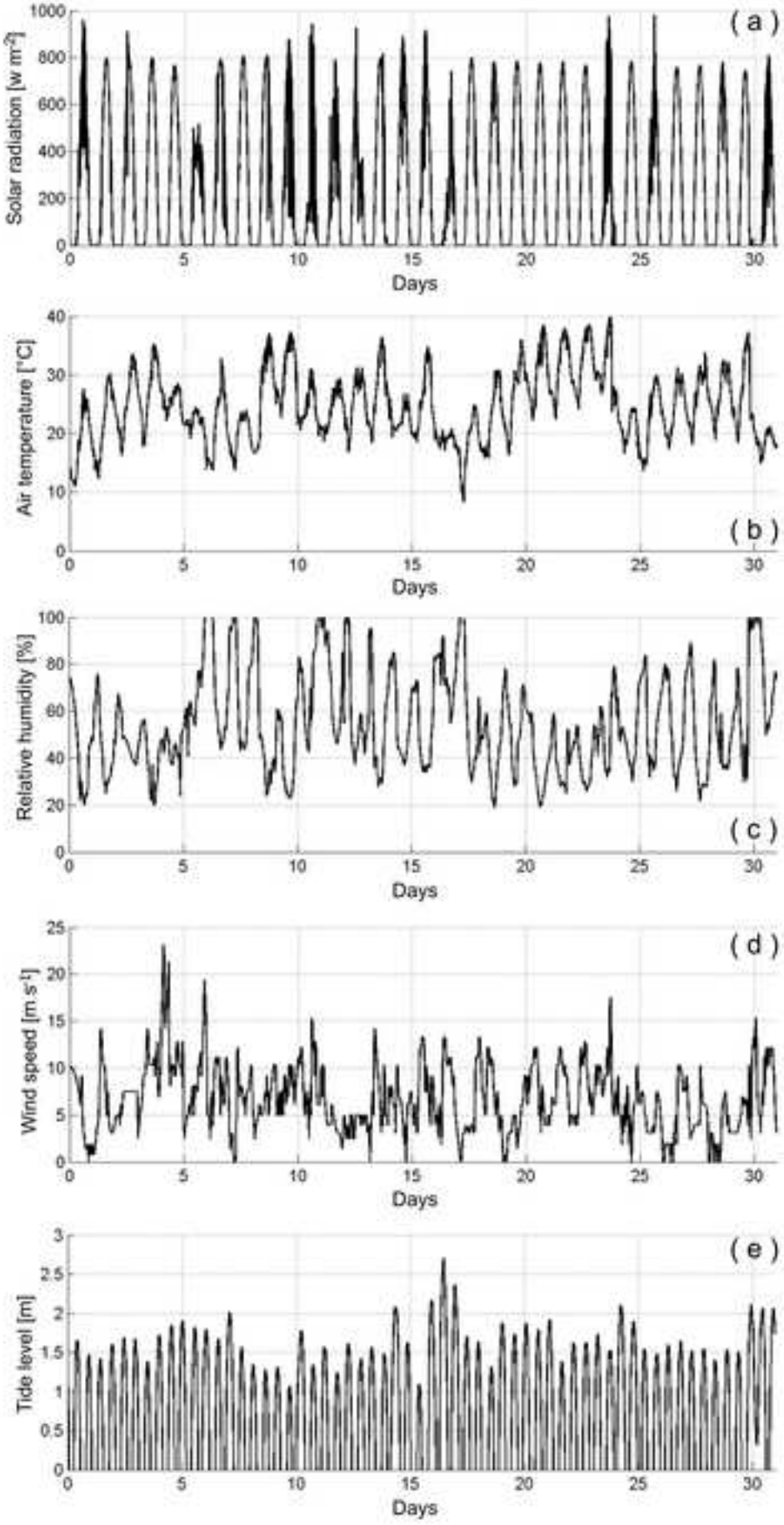

colour figure-6
Click here to download high resolution image

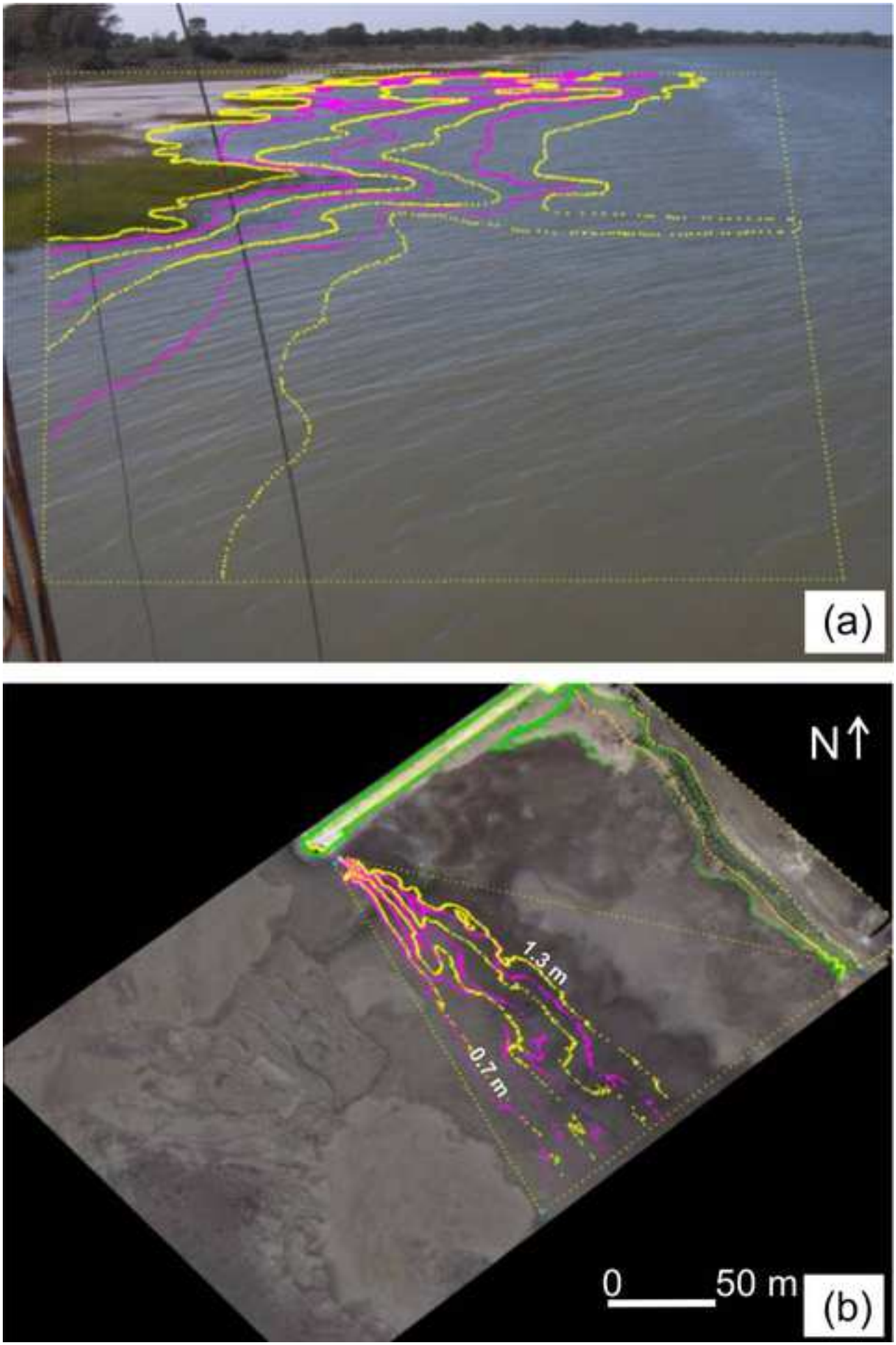

colour figure-7
Click here to download high resolution image

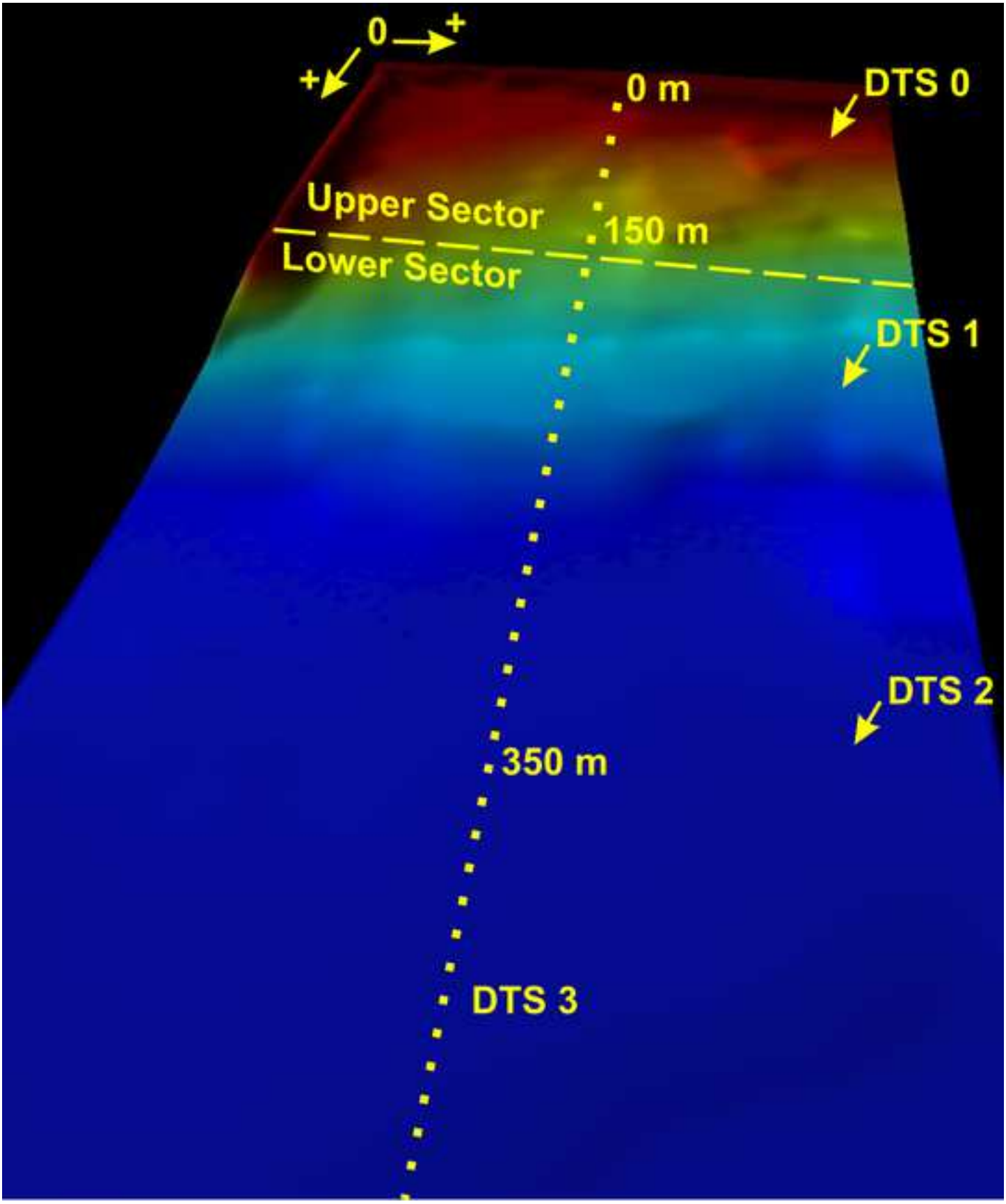

line figure-8
Click here to download high resolution image

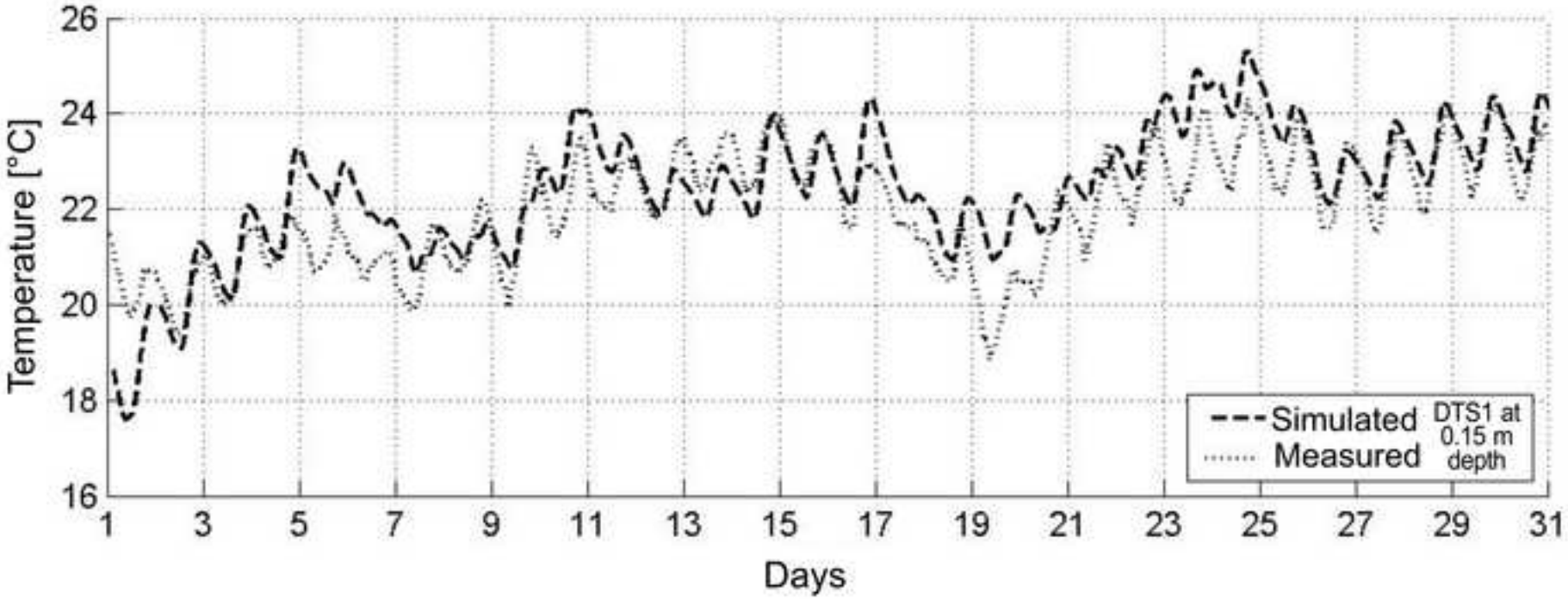

line figure-9
Click here to download high resolution image

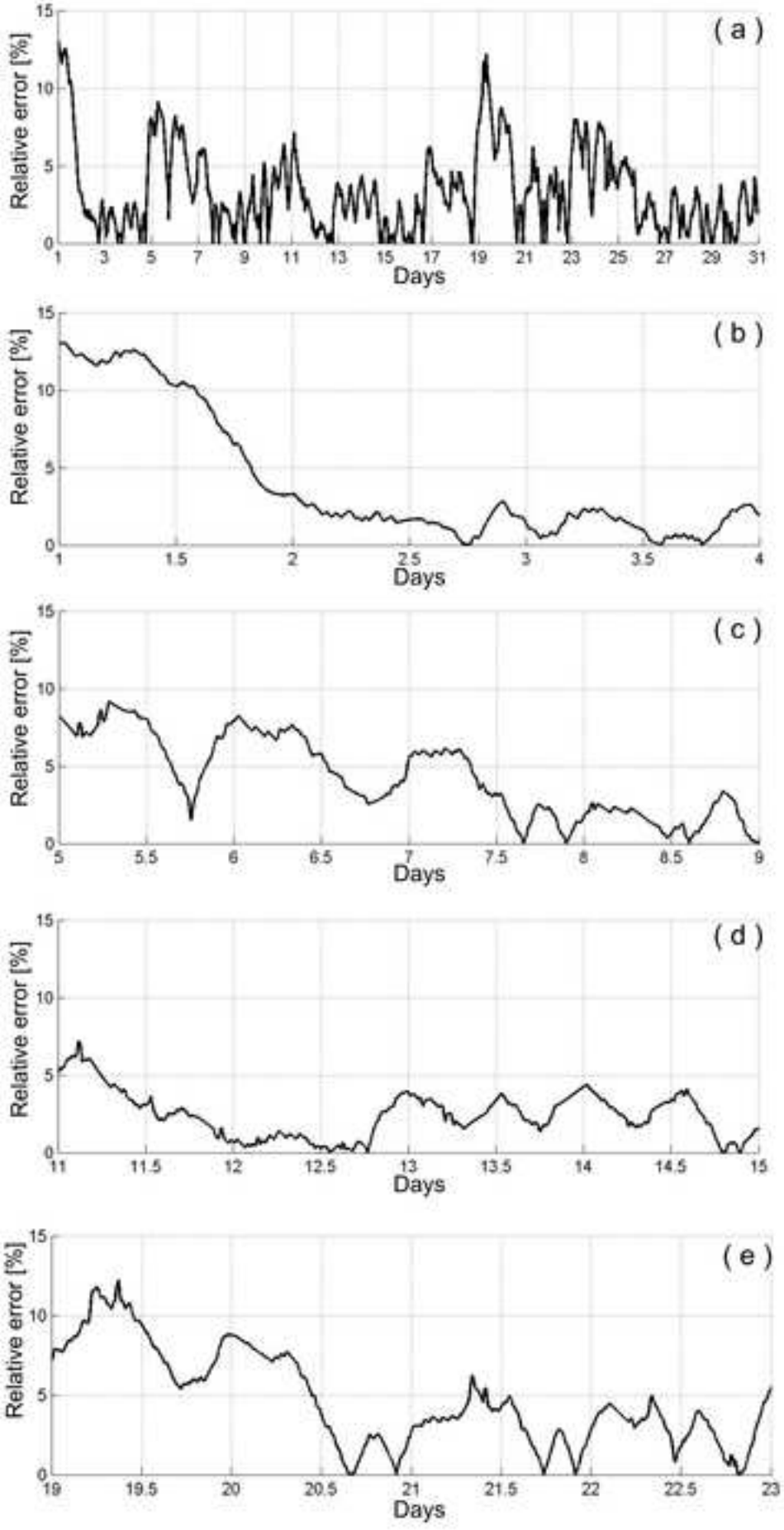

colour figure-10
Click here to download high resolution image

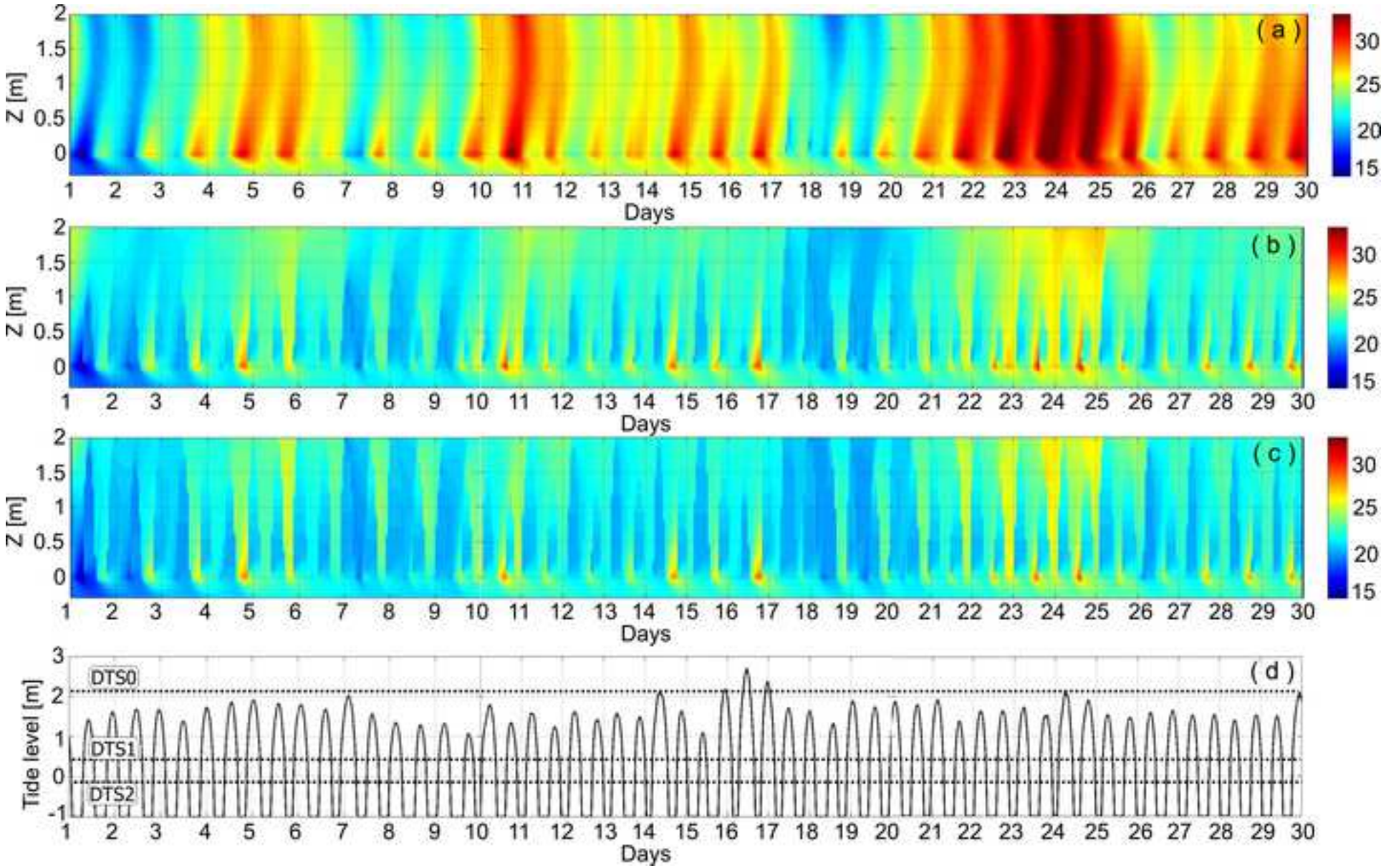

colour figure-11
Click here to download high resolution image

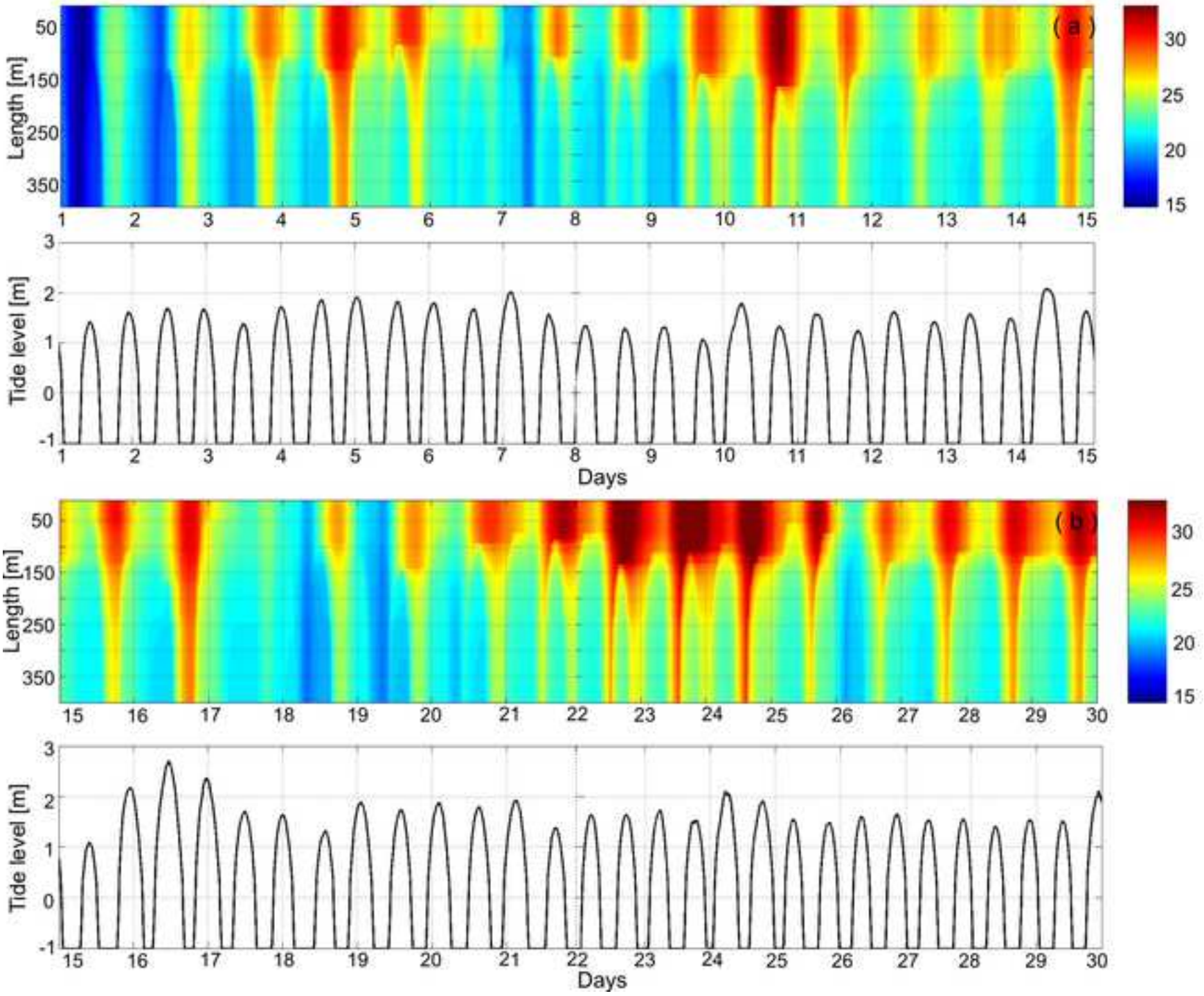

line figure-12
Click here to download high resolution image

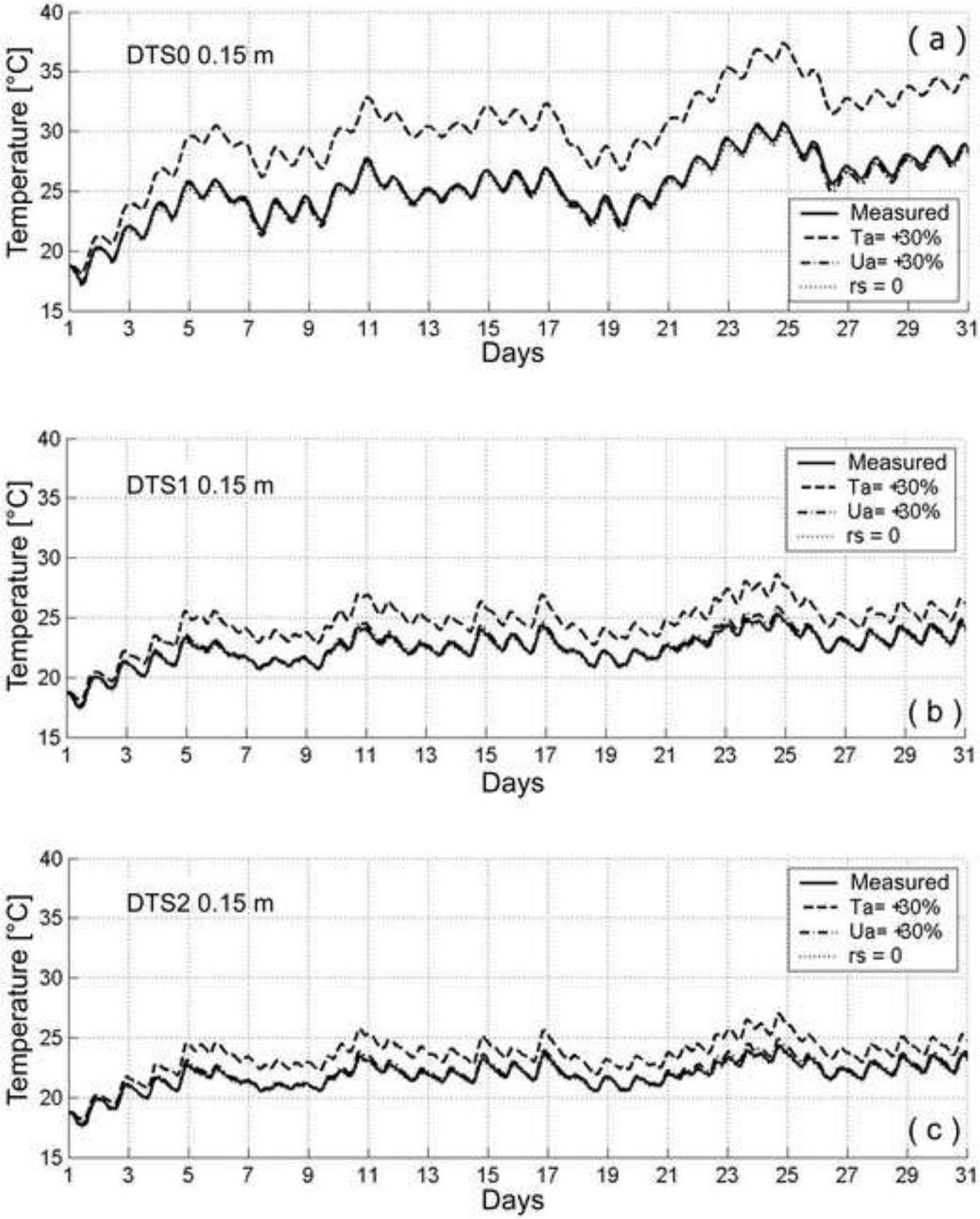

colour figure-13
Click here to download high resolution image